AIAA JOURNAL
Vol. 32, No. 2, February 1994

Sensitivity Analysis of Aeroelastic Response of a Wing in Transonic Flow

Rakesh K. Kapania* and Jason Cherian Issac†
Virginia Polytechnic Institute and State University, Blacksburg, Virginia 24061

A sensitivity study of the aeroelastic response of a wing in transonic flow is carried out for changes in shape parameters, namely, aspect ratio, surface area of the wing, taper ratio, and sweep. The structural model is based on a Ritz solution technique with wing deflections represented by Chebyshev polynomials. A recently developed compressible aerodynamic state-space model is used to represent the unsteady aerodynamic airloads on the wing. The aeroelastic equations are solved as an eigenvalue problem to determine the critical speed of the wing. The derivatives of the flutter and divergence speeds with respect to the shape parameters are calculated by both analytical and finite difference methods. The shape sensitivity derivatives give a linear approximation to the critical speed curves over a range of values of the shape parameter which is perturbed.

Introduction

STUDIES on aeroelastic instabilities, namely, flutter and divergence, in transonic flow are important in the design of aircraft that operate in the transonic regime. Moreover, as compressibility effects are very important in transonic flow, a compressible aerodynamic theory must be used to model the unsteady aerodynamic behavior. It is important to obtain information about the dependence of aeroelastic instability on the design parameters of the wing through a sensitivity analysis.

In recent years, considerable efforts are being made to integrate the aerodynamic, structural, and control aspects of the design of an aircraft. It is desirable that the unsteady aerodynamic airloads be expressed in a state-space form. Leishman and Nguyen[1] have represented the aerodynamic indicial response functions for compressible flow by up to three-pole approximations, the response consisting of two parts, one due to noncirculatory loading and the other due to circulatory loading. Using this approach, the aeroelastic equations can be written as a set of first-order ordinary differential equations as given by Leishman and Crouse.[2] This has advantages over the CFD-based methods in the sense that the CFD methods are in general computationally very expensive.

Sensitivity analysis is becoming an important design tool in engineering design applications. Sensitivity derivatives are of great importance in multidisciplinary design optimization of aircraft. Sobieszczanski-Sobieski[3] discusses in detail the system design derivatives that help in understanding the effect a particular design variable would have on the desired performance of the system, if it were perturbed by a small percentage from its original value.

The sensitivity derivatives of a system can be found using either analytical or finite difference methods. Analytical sensitivity analysis has found increased interest in engineering design as it eliminates uncertainity in the choice of step size needed in the finite difference method. The step size if too large leads to truncation errors and if too small leads to round-off errors. For example, recently Livne[4] observed that as higher order polynomials are used in the Ritz functions for better modeling of the structure, the more sensitive is the finite difference derivative to the step size used, and in some cases it is impossible to obtain any valuable information by finite differences.

Rudisill and Bhatia[5] developed expressions for the analytical derivatives of the eigenvalues, reduced frequency, and flutter speed with respect to structural parameters for use in minimizing the total mass. Pedersen and Seyranian[6] examined the change in flutter load as a function of change in stiffness, mass, boundary conditions, or load distribution. They showed how sensitivity analysis can be performed without any new eigenvalue analysis. The solution to the main and an adjoint problem provide all the necessary information for evaluating sensitivities.

Hawk and Bristow[7] developed aerodynamic sensitivity analysis capabilities in subcritical compressible flow. They first analyzed a baseline configuration, and then calculated a matrix containing partial derivatives of the potential at each control point with respect to each known geometric parameter by applying a first-order expansion to the baseline configuration. The matrix of partial derivatives is used in each iteration cycle to analyze the perturbed geometry. However, this analysis only handles chordwise perturbation distributions, such as changes in camber, thickness, and twist. A new approach, which is still under development, has been presented by Yates[8] that considers general geometric variations, including planform, and subsonic, sonic, and supersonic unsteady, nonplanar lifting-surface theory.

Barthelemy and Bergen[9] explored the analytical shape sensitivity derivatives of the wing's aeroelastic characteristics, such as section lift, angle of attack, rolling moment, induced drag, and divergence dynamic pressure, for subsonic subcritical flow, with respect to geometric parameters. Results showed the characteristics nonlinearity to be small enough to be well approximated by sensitivity-based linear approximations. These approximations are valid within a range that is useful to designers in the initial design phase. Kapania[10] has obtained sensitivity derivatives of the flutter speed of a two-dimensional airfoil in incompressible flow with respect to the mass and stiffness parameters. Kapania, Bergen, and Barthelemy[11] have obtained the shape sensitivity derivatives of the flutter response of a laminated wing in incompressible flow.

In this paper, the aerodynamic state-space model[1] is used to represent the unsteady aerodynamic airloads on a wing. The wing structure is modeled as a wing box and Chebyshev polynomials are chosen for the displacement function. The aeroelastic equations for the wing are solved as an eigenvalue problem to determine the stability. The derivatives of the critical speed are calculated with respect to the shape parameters, namely, aspect ratio, area, taper ratio, and sweep, by analytical and finite-difference methods. To the best of our knowledge, this is a first study on the sensitivity analysis of the aeroelastic response in transonic flow.

Presented as Paper 93-1646 at the AIAA/ASME/ASCE/AHS/ASC 34th Structures, Structural Dynamics, and Materials Conference, La Jolla, CA, April 19–21, 1993; received May 10, 1993; revision received Aug. 13, 1993; accepted for publication Aug. 13, 1993.

*Associate Professor, Aerospace and Ocean Engineering. Associate Fellow AIAA.

†Graduate Research Assistant, Aerospace and Ocean Engineering. Student Member AIAA.

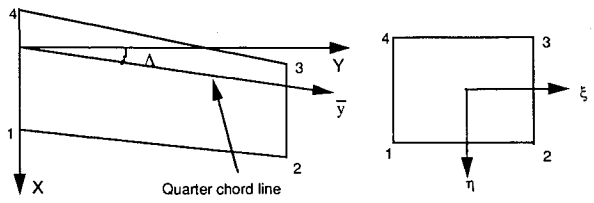

Fig. 1 Original and transformed coordinate systems.

Aerodynamic Model

In recent years, considerable efforts are being made to integrate the aerodynamic, structural, and control aspects of the design of an aircraft. Since the control and the structural dynamic behaviors can easily be expressed in the state-space form (i.e., in terms of a set of first-order ordinary differential equations in time), it is desirable that the unsteady aerodynamic airloads be also expressed in the same form. In recent years, considerable efforts have been made in that direction.

The state-space approach has the advantage that any system of differential equations can be represented by a set of first-order ordinary differential equations of the form

$$\dot{\boldsymbol{x}} = \boldsymbol{A}\boldsymbol{x} + \boldsymbol{B}\boldsymbol{u} \tag{1}$$

with the output equations given by

$$\boldsymbol{y} = \boldsymbol{C}\boldsymbol{x} + \boldsymbol{D}\boldsymbol{u} \tag{2}$$

where $\boldsymbol{x}$ are the aerodynamic state variables, $\boldsymbol{u}$ are the system inputs, and $\boldsymbol{y}$ are the system outputs. If the unsteady aerodynamic behavior can be represented by state equations, then they can be easily coupled to the structural equations of motion and the resulting system can be examined for aeroelastic stability.

In this paper, the state-space representation given by Leishman and Nguyen[1] has been used to represent the compressible unsteady aerodynamics. The indicial normal force and quarter chord pitching moment responses to a step change in angle of attack α and a step change in pitch rate q can be written as[1]

$$\frac{C_N(S)}{\alpha} = \frac{4}{M}\phi_\alpha^I(S,M) + C_{N_\alpha}(M)\,\phi_\alpha^C(S,M)$$

$$\frac{C_M(S)}{\alpha} = -\frac{1}{M}\phi_{\alpha M}^I(S,M) + C_{N_\alpha}(M)\,\phi_\alpha^C(S,M)\,[0.25 - x_{ac}(M)] \tag{3}$$

$$\frac{C_N(S)}{q} = \frac{1}{M}\phi_q^I(S,M) + \frac{C_{N_\alpha}(M)}{2}\phi_q^C(S,M)$$

$$\frac{C_M(S)}{q} = -\frac{7}{12M}\phi_{qM}^I(S,M) - \frac{C_{N_\alpha}(M)}{16}\phi_{qM}^C(S,M)$$

where ϕ_α^C, ϕ_α^I, $\phi_{\alpha M}^I$, ϕ_q^C, ϕ_q^I, ϕ_{qM}^C, ϕ_{qM}^I are exponential functions of S and M. Here, M is the Mach number, $S = 2Vt/c$, V the freestream velocity, t the time, and c the chord; $q = \dot{\alpha}\,c/V$ is the pitch rate, C_N is the normal force coefficient, C_M is the pitching moment coefficient about the quarter chord, and C_{N_α} the normal force curve slope. The superscripts C and I refer to circulatory and noncirculatory components of the indicial response functions. Note that $2\pi/\beta$ (where $\beta = \sqrt{1-M^2}$ is the compressibility factor) in Ref. 1 has been replaced by $C_{N_\alpha}(M)$, so that experimental values of C_{N_α} obtained as functions of Mach number can be used.

The aerodynamic state equations have been shown by Leishman and Nguyen[1] to be given by

$$\dot{\boldsymbol{x}} = \boldsymbol{A}\boldsymbol{x} + \boldsymbol{B}\begin{Bmatrix}\alpha\\ q\end{Bmatrix} \tag{4}$$

where

$$\boldsymbol{A} = \text{diag}\,[a_{11}\ a_{22}\ a_{33}\ a_{44}\ a_{55}\ a_{66}\ a_{77}\ a_{88}]$$

$$\boldsymbol{B} = \begin{bmatrix}1 & 1 & 1 & 0 & 1 & 1 & 0 & 0\\ 0.5 & 0.5 & 0 & 1 & 0 & 0 & 1 & 1\end{bmatrix}^T$$

The output equations are given by

$$\begin{Bmatrix}C_N\\ C_M\end{Bmatrix} = \boldsymbol{C}\boldsymbol{x} + \boldsymbol{D}\begin{Bmatrix}\alpha\\ q\end{Bmatrix} \tag{5}$$

where

$$\boldsymbol{C} = \begin{bmatrix}c_{11} & c_{12} & c_{13} & c_{14} & 0 & 0 & 0 & 0\\ c_{21} & c_{22} & 0 & 0 & c_{25} & c_{26} & c_{27} & c_{28}\end{bmatrix}$$

$$\boldsymbol{D} = \begin{bmatrix}4/M & 1/M\\ -1/M & -7/12M\end{bmatrix}$$

The nonzero terms of the a_{ij} and c_{ij} are given in Ref. 12.

Aeroelastic Analysis of the Wing

Structural Model

The structural formulation is based on a Ritz solution technique using the energy functionals for a laminated plate, which includes the bending and stretching of the reference surface. The planform geometry can be represented by any generally tapered, skewed configuration. The original rectangular (x, y) coordinate system and the transformed (η, ξ) coordinate system of the wing are shown in Fig. 1. The x-y plane is the midplane of the wing and the z axis is normal to the wing. For an unswept wing the fiber angle is measured counterclockwise from the positive y axis. As the wing is swept, the fiber angle is also rotated correspondingly.

In the Rayleigh-Ritz formulation, Chebyshev polynomials T_i are used to represent the displacements at any point on the wing.[13] The Chebyshev polynomials are given by

$$T_0(\psi) = 1$$

$$T_1(\psi) = \psi \tag{6}$$

$$T_i(\psi) = 2\psi T_{i-1} - T_{i-2}, \qquad -1 \le \psi \le 1$$

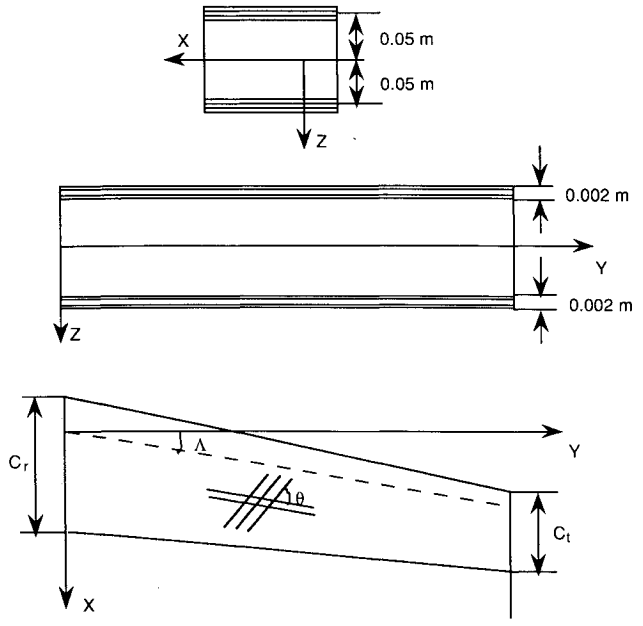

Fig. 2 Critical speed vs sweep angle, aspect ratio = 10, area = 20 m², taper ratio = 0.5.

The displacements are expressed in terms of the Chebyshev polynomials as shown

$$U(\eta,\xi) = \sum_{i=0}^{I}\sum_{j=0}^{J} R_{ij}T_i(\eta)T_j(\xi)$$

$$V(\eta,\xi) = \sum_{k=0}^{K}\sum_{l=0}^{L} S_{kl}T_k(\eta)T_l(\xi) \tag{7}$$

$$W(\eta,\xi) = \sum_{m=0}^{M}\sum_{n=0}^{N} P_{mn}T_m(\eta)T_n(\xi), \qquad -1 \le \eta, \xi \le 1$$

It has been shown by Kapania and Singhvi[13] that for free vibrations of the laminated composite wing (i.e., in the absence of aerodynamic forces) the equations of motion can be derived using classical plate theory in the form $[M]\{\ddot{q}\} + [\bar{K}]\{q\} = 0$ where $[\bar{K}]$ and $[M]$ are the stiffness and mass matrices. The eigenvector $\{q\}$ is defined as $\{q\} = (R_{00}, R_{01}, \ldots R_{ij}; S_{00}, S_{01}, \ldots S_{kl}; P_{00}, P_{01}, \ldots P_{mn})^T$. Linear and rotational springs of large magnitude are placed at the wing root to satisfy the clamped boundary conditions. The stiffness matrix for the plate alone (i.e., excluding the springs) is

$$[\bar{K}] = \int_{-1}^{1}\int_{-1}^{1} [\bar{B}]^T [T]^T \begin{bmatrix} A & B \\ B & D \end{bmatrix} [T] [\bar{B}] |J| \, d\eta \, d\xi \tag{8}$$

and a typical element of the mass matrix $[M]$ is given by

$$M_{ij} = \rho_m t \int_{-1}^{1}\int_{-1}^{1} T_k(\eta)T_l(\xi)T_p(\eta)T_r(\xi)|J| \, d\eta \, d\xi \tag{9}$$

where ρ_m is the material density, t is the thickness of the plate, and $k = 0, 1, 2, \ldots, K$, $l = 0, 1, 2, \ldots, L$, $p = 0, 1, 2, \ldots, K$, $r = 0, 1, 2, \ldots, L$ for $1 \le i,j \le (K+1)(L+1)$. The mass matrix $[M]$ is then of order $(K+1)(L+1)$. The details of the $[T]$ and $[\bar{B}]$ matrices and J are given in Ref. 14. The coefficients R_{ij} and S_{kl} in $\{q\}$ corresponding to the inplane displacements are condensed out using static condensation to the form

$$[M]\{\ddot{P}_{mn}\} + [K]\{P_{mn}\} = 0 \tag{10}$$

where $[M]$ is the mass matrix and $[K]$ is the stiffness matrix of order $(m+1)(n+1)$ with generalized displacements $\{P_{mn}\}$.

Aeroelastic Model

The aerodynamic state-space model that was used for the aeroelastic analysis of a typical section in Ref. 2 is extended to represent the unsteady aerodynamic forces acting on a wing in transonic flow. The lift and moment forces per unit span on a typical section acting at the quarter chord are given as $L = 1/2\rho V^2 c C_N$ and $M = 1/2\rho V^2 c^2 C_M$.

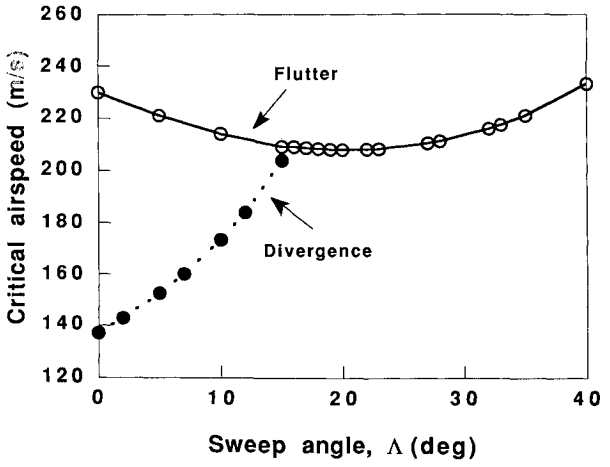

Fig. 3 Critical speed vs sweep angle, aspect ratio = 10, area = 20 m², taper ratio = 0.5.

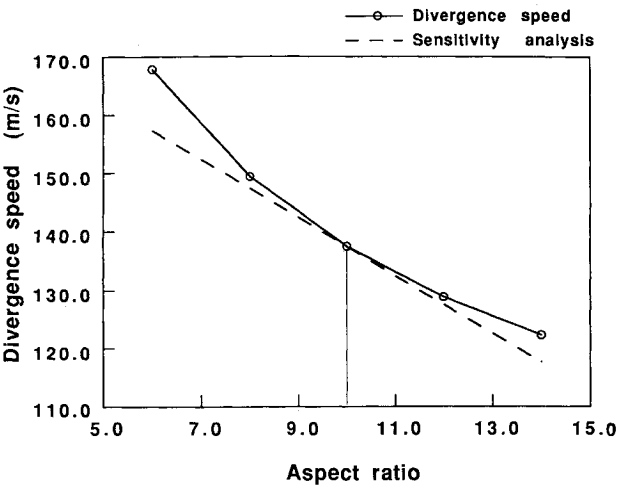

Fig. 4 Divergence speed vs aspect ratio (M = 0.9), aspect ratio = 10, area = 20 m², taper ratio = 0.5, sweep = 0 deg.

When extending this two-dimensional compressible aerodynamic theory to a finite span wing, the lift forces are assumed to be distributed along the quarter chord line (reference line) and the moments act about the reference line. Since the lift and moment forces are nonconservative forces, using the principle of virtual work, we get

$$\delta W_{nc} = \int_0^l -L\delta h \, d\bar{y} + \int_0^l M\delta\theta \, d\bar{y} \tag{11}$$

where l is the length of the quarter chord line, δh and $\delta\theta$ are virtual displacement and rotation, respectively, and $\bar{y}$ is the coordinate along the reference line.

The displacement at any location $\bar{y}$ along the reference line is given by

$$h(\bar{y}) = w(\eta, \xi) \tag{12}$$

where η and ξ are the natural coordinates corresponding to the (x, y) coordinates of the point at distance $\bar{y}$ from the origin.

The rotation about the reference line (positive wing leading edge up) is given by

$$\theta(\bar{y}) = w_{,x} \cos\Lambda - w_{,y} \sin\Lambda \tag{13}$$

For facilitating in numerical integration using Gaussian quadrature, the limits of integration along the reference line are transformed in the range of -1 to 1 by $\bar{y} = l(1+\psi)/2$, where $-1 \le \psi \le 1$.

Substituting the expressions for the lift and moment on the wing and the wing deflection, we have

$$\int_0^l L\delta h \, d\bar{y} = \frac{l}{2}\int_{-1}^{1} L\delta h \, d\psi$$

$$= \frac{l}{2}\left(\frac{1}{2}\rho V^2\right)\sum_{i=0}^{m}\sum_{j=0}^{n}\left[\int_{-1}^{1} c\left([C_{1p}]\{x\} + [D_{1p}]\begin{bmatrix} H_{ij} & 0 \\ 0 & H_{ij} \end{bmatrix}\begin{Bmatrix} P_{ij} \\ \dot{P}_{ij} \end{Bmatrix}\right) w_{1_{ij}} \, d\psi\right]\delta P_{ij}$$

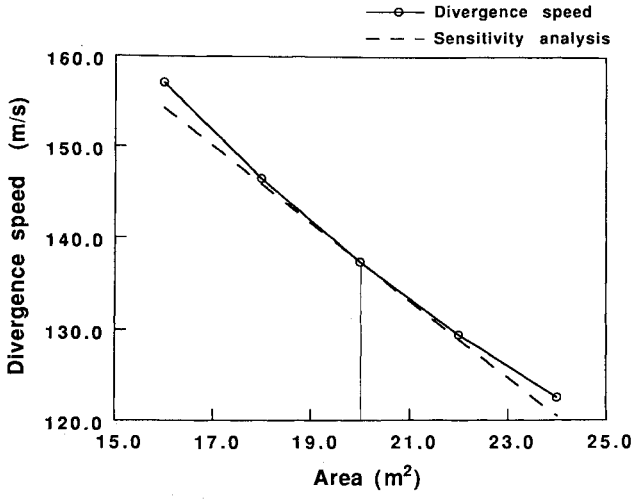

Fig. 5 Divergence speed vs area (M = 0.9), aspect ratio = 10, area = 20 m², taper ratio = 0.5, sweep = 0 deg.

and

$$\int_0^l M\delta\theta\, d\bar{y} = \frac{l}{2}\int_{-1}^{1} M\delta\theta\, d\psi$$

$$= \frac{l}{2}\left(\frac{1}{2}\rho V^2\right)\sum_{i=0}^{m}\sum_{j=0}^{n}\left[\int_{-1}^{1} c^2\left([C_{2p}]\{x\} + [D_{2p}]\begin{bmatrix} H_{ij} & 0 \\ 0 & H_{ij} \end{bmatrix}\begin{Bmatrix} P_{ij} \\ \dot{P}_{ij} \end{Bmatrix}\right) w_{2_{ij}}\, d\psi\right]\delta P_{ij} \tag{14}$$

where m and n represent the order of the Chebyshev polynomial used in the displacement function. The row vectors $[C_{1p}]$ and $[C_{2p}]$ are the elements of the $[C]$ matrix (see section on aerodynamic model) where $p = 1, 2, \ldots, 8$. The row vectors $[D_{1p'}]$ and $[D_{2p'}]$ are the elements of the matrix given by

$$[D] = \begin{bmatrix} 4/M & 1/M \\ -1/M & -7/12M \end{bmatrix}\begin{bmatrix} 0 & 1 & 1/V & 0 \\ 0 & 0 & 0 & c/V \end{bmatrix} \tag{15}$$

where $p' = 1, \ldots, 4$.

The variables $w_{1_{ij}}$ and $w_{2_{ij}}$ in Eq. (14) are given by

$$w_{1_{ij}} = T_i(\eta)T_j(\xi)$$
$$w_{2_{ij}} = \cos\Lambda(T_{i,\eta}T_j\eta_{,x} + T_iT_{j,\xi}\xi_{,x}) - \sin\Lambda(T_{i,\eta}T_j\eta_{,y} + T_iT_{j,\xi}\xi_{,y}) \tag{16}$$

where Λ is the sweep angle.

$[H_{ij}]$ in Eq. (14) is a matrix of order $2 \times N$ where $N = (m + 1)(n + 1)$. A typical column of the matrix is given by

$$H_k = \begin{Bmatrix} w_{1_{ij}} \\ w_{2_{ij}} \end{Bmatrix} \tag{17}$$

where $k = 1, 2, \ldots, N$ and w_{1ij} and w_{2ij} are given by Eq. (16).

The column vector $\{x\}$ in Eq. (14) is the vector of aerodynamic state variables and $\{P_{ij}\dot{P}_{ij}\}^T$ is the vector of generalized displacements.

It should be noted that in the integrations performed along the quarter-chord line in Eq. (14), a constant value of the section lift-curve slope C_{N_α} is used along the span. But for a three-dimensional finite wing, the wing lift-curve slope depends on the planform of the wing which makes C_{N_α} sensitive to shape variations of the wing, which is not addressed in the present study.

Using Eqs. (12–14), Eq. (11) can be written as

$$\delta W_{nc} = \sum_{i=1}^{N} Q_i \delta P_i \tag{18}$$

where $N = (m + 1)(n + 1)$ and

$$Q_i = [C']\{x\} + [D'_1\ D'_2]\begin{Bmatrix} P_{ij} \\ \dot{P}_{ij} \end{Bmatrix} \tag{19}$$

The aerodynamic state Eqs. (4) for a typical section perpendicular to the quarter chord line were in the form

$$\{\dot{x}\} = [A]\{x\} + [B]\{u\}$$

An integration of these state equations along the quarter chord line to consider the effect of finite span yields

$$\{\dot{x}\} = \frac{1}{2}\int_{-1}^{1}\left([A]\{x\} + [B]\begin{bmatrix} H_{ij} & 0 \\ 0 & H_{ij} \end{bmatrix}\begin{Bmatrix} P_{ij} \\ \dot{P}_{ij} \end{Bmatrix}\right) d\psi$$

$$= [A']\{x\} + [B'_1\ B'_2]\begin{Bmatrix} P_{ij} \\ \dot{P}_{ij} \end{Bmatrix} \tag{20}$$

Equation (10) can be written as a set of first order ODEs in $\{P_{ij}\}$ and $\{\dot{P}_{ij}\}$ which will be represented by $\{p_i\}$ and $\{q_i\}$, re-

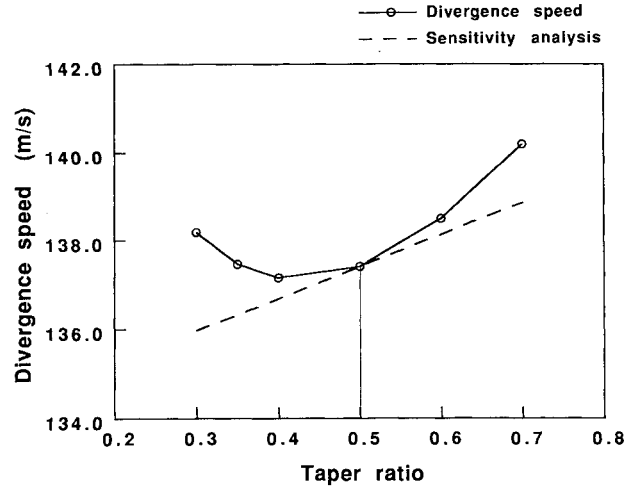

Fig. 6 Divergence speed vs taper ratio (M = 0.9), aspect ratio = 10, area = 20 m², taper ratio = 0.5, sweep = 0 deg.

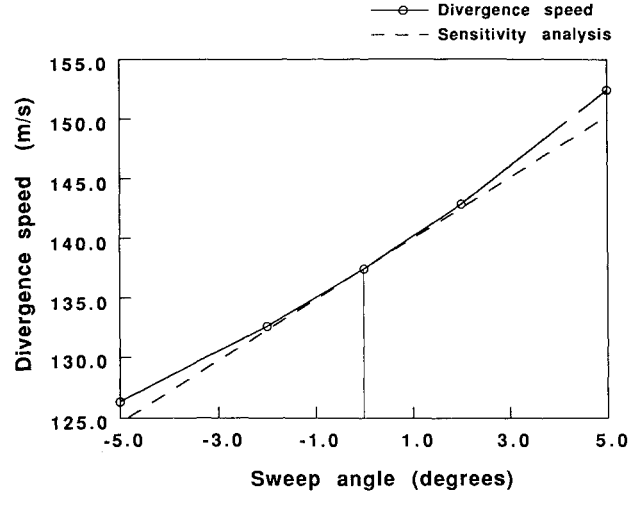

Fig. 7 Divergence speed vs sweep angle (M = 0.9), aspect ratio = 10, area = 20 m², taper ratio = 0.5, sweep = 0 deg.

Table 1 Comparison of natural frequencies of an unswept wing and its flutter speed in subsonic flow[a]

Laminate sequence	Present				Dugundi and Landsberger[15]			
	Natural frequencies, Hz			Flutter speed,	Natural frequencies, Hz			Flutter speed,
	First	Second	Third	m/s	First	Second	Third	m/s
$[0_2/90]_s$	11.03	39.30	69.06	24.9	10.8	39	67	26
$[15_2/0]_s$	8.86	42.62	63.25	23.2	8.5	48	58	25
$[\pm 15/0]_s$	10.12	48.90	64.94	28.1	9.9	50	63	28
$[\mp 15/0]_s$	10.12	48.90	64.94	18.9	9.9	50	63	21
$[+30/0]_s$	6.21	37.57	57.78	28.8	6.0	41	60	29

[a]Area = 0.02318 m^2, aspect ratio = 4.0132, taper ratio = 1.0.

Table 2 Comparison of flutter speed of the 2.5 ft WEAK3 model with flutter data measured in the transonic wind tunnel[a]

Mach number, M	Mass ratio, μ	Density of air (slugs/ft^3)	Flutter speed, V (ft/s)	Nondimensional speed $V/(b_s\omega_\alpha\sqrt{\mu})$	
				Present	Experimental[16]
0.499	33.465	0.000830	476.90	0.3896	0.4459
0.678	68.753	0.000404	640.00	0.3647	0.4174
0.901	143.92	0.000193	829.44	0.3267	0.3700

[a]Area = 3.782 ft^2, aspect ratio = 1.6525, taper ratio = 0.6576, sweep = 45 deg.

spectively. It can be coupled with Eqs. (19) and (20) to generate the aeroelastic equations of the wing in the form

$$\begin{bmatrix} I & 0 & 0 \\ 0 & M & 0 \\ 0 & 0 & I \end{bmatrix} \begin{Bmatrix} \dot{p}_i \\ \dot{q}_i \\ \dot{x} \end{Bmatrix} = \begin{bmatrix} 0 & I & 0 \\ D_1' & -K & D_2' & C' \\ B_1' & & B_2' & A' \end{bmatrix} \begin{Bmatrix} p_i \\ q_i \\ x \end{Bmatrix} \tag{21}$$

Since a Chebyshev polynomial of order five is chosen for the displacement function in both η and ξ, we have 36 generalized displacements $\{p_i\}$, their 36 time derivatives $\{q_i\}$ and the eight aerodynamic state variables $\{x\}$. The stability of this system can be determined by solving an 80×80 eigenvalue problem.

Sensitivity Analysis

The aeroelastic equations obtained as a set of first-order ODEs is of the form

$$[P]\dot{w} = [Q]w \tag{22}$$

which could be written as

$$\dot{w} = [E]w \tag{23}$$

where $[E] = [P]^{-1}[Q]$

The derivative of the ith eigenvalue with respect to the critical speed is given by

$$\frac{\partial \lambda^i}{\partial \nabla f} = \frac{\{e_l^i\}^T (\partial [E]/\partial V_f) \{e_r^i\}}{\{e_l^i\}^T \{e_r^i\}} \tag{24}$$

where $\{e_l^i\}$ and $\{e_r^i\}$ are the ith left and right eigenvectors, respectively.

Similarly, the derivative of the ith eigenvalue with respect to any parameter p is given by

$$\frac{\partial \lambda^i}{\partial p} = \frac{\{e_l^i\}^T (\partial [E]/\partial p) \{e_r^i\}}{\{e_l^i\}^T \{e_r^i\}} \tag{25}$$

$(\partial [E]/\partial p)$ can be conveniently written as

$$\frac{\partial [E]}{\partial p} = \frac{\partial [P]^{-1}}{\partial p}[Q] + [P]^{-1}\frac{\partial [Q]}{\partial p} \tag{26}$$

and can be computed analytically, where

$$\frac{\partial [P]^{-1}}{\partial p} = -[P]^{-1}\frac{\partial [P]}{\partial p}[P]^{-1} \tag{27}$$

The analytical derivative of the critical speed with respect to parameter p is then given by

$$\frac{\partial V_f}{\partial p} = -\frac{\text{Real}\,(\partial \lambda^i/\partial p)}{\text{Real}\,(\partial \lambda^i/\partial V_f)} \tag{28}$$

The $[E]$ matrix is composed of mass, stiffness, and aerodynamic matrices. The expressions for the analytical derivatives of the $[\bar{K}]$ and $[M]$ matrices [Eqs. (8) and (9)] are given in Ref. 14. Since the reduced stiffness matrix $[K]$ is obtained from $[\bar{K}]$ by static condensation the analytical derivative $\partial[K]/\partial p$ is obtained by a succession of differentiations using the chain rule. The derivatives of the aerodynamic terms are obtained by taking the analytical derivatives of those terms that are explicit functions of the shape parameters which are given in Ref. 12.

Evaluation Analysis

Sensitivity calculations of the flutter speed of a typical section with respect to mass ratio (μ), static unbalance (x_θ), radius of gyration (r_θ), uncoupled bending frequency (ω_h) and uncoupled torsion frequency (ω_θ) were first performed. The results of these studies are given in Ref. 12.

Before performing the sensitivity calculations of the critical speed of the wing with respect to shape parameters, comparison of natural frequencies and predicted flutter speeds was made with results from other sources. The first three natural frequencies of an unswept wing and its flutter speed in subsonic flow were compared with results reported by Dugundji and Landsberger[15] for different laminate sequences in Table 1. The material used for the wing is Hercules Graphite Epoxy (AS1/3501-6) with properties: $E_1 = 98 \times 10^9$ Pa, $E_2 = 7.9 \times 10^9$ Pa, $\nu_{12} = 0.28$, $G_{12} = 5.6 \times 10^9$ Pa, and $\rho = 1520$ kg/m^3. The thickness of each ply is 0.134×10^{-3} m. The flutter data used for comparison[15] are the experimental results from the wind tunnel tests performed in the Massachusetts Institute of Technology (MIT) acoustic wind tunnel. The results agree fairly well.

An experimental investigation of the flutter characteristics of the wing in transonic flow was performed in the Langley transonic dynamics tunnel, the results of which have been reported by Yates.[16] The 2.5 ft WEAK3 model is used for comparison with our results. The material properties of the laminated mahogany wing are: $E_1 = 0.47072 \times 10^6$ psi, $E_2 = 0.01883 \times 10^6$ psi, $\nu_{12} = 0.28$, $G_{12} = 0.05975 \times 10^6$ psi, and $\rho = 0.60267$ slugs/ft^3. The wing dimensions are: area = 3.782 ft^2, aspect ratio = 1.6525, taper ratio = 0.6576, sweep (1/4 chord) = 45 deg, and thickness = 0.056 ft. The first four natural frequencies obtained from the present analysis were 9.91, 36.75, 60.78, and 102.11 Hz compared to the experimental values of 9.60, 38.10, 50.70, and 98.50, respectively, presented in Ref. 16. The flutter speed obtained from this analysis is compared with the nondimensional flutter data measured in air for the WEAK3 model[16] at different Mach numbers in Table 2. The nondimensionalizing parameter used is $b_s\omega_\alpha\sqrt{\mu}$ where μ is the mass ratio, b_s is the root semichord, and ω_α is the angular fre-

quency of the first torsion mode. For this model, b_s and w_α are 0.9165 ft and 230.9 rad/s, respectively. It should be noted that the 2.5 ft WEAK3 model has a low aspect ratio of 1.6525. In our aerodynamic model, we have assumed the lift forces to be acting along the quarter chord line and the moments about the quarter chord line, which is a good assumption for high-aspect- ratio wings. In reality however, the aerodynamic forces and moments are distributed over the surface of the wing. Yet, the flutter results obtained are encouraging.

Having achieved good prediction of flutter speeds, sensitivity analysis of the flutter speed of the wing with respect to shape parameters is carried out. The wing box is shown in Fig. 2. The wing skins are made of 0 deg laminated Graphite/Epoxy (T300/N5208) with the following material properties: $E_1 = 181 \times 10^9$ Pa, $E_2 = 10.3 \times 10^9$ Pa, $\nu_{12} = 0.28$, $G_{12} = 7.17 \times 10^9$ Pa, and $\rho = 1600$ kg/m^3. The critical airspeed of the wing is shown in Fig. 3 as a function of the quarter chord sweep angle. As seen from the graph, divergence (zero-frequency flutter) instability is critical up to a sweep angle of about 16 deg and for higher sweep angles, the flutter mode is the unstable mode. Tables 3 and 4 give the shape sensitivity derivatives of the divergence speeds and flutter speeds of a wing at Mach 0.9. The analytical shape derivatives agree well with the finite difference derivatives obtained using different step sizes.

The critical speeds of the wing obtained by perturbing one shape parameter at a time from the baseline configuration are shown in Figs. 4–11. The prediction of critical speed by analytical sensitivity calculations is also superposed. The sensitivity derivative obtained forms a tangent to the critical speed curve at the value of the shape parameter at which it is computed.

It is observed from Figs. 4 and 8 that the divergence and flutter speeds, respectively, drop as the aspect ratio increases. Physically, as the wing is made more slender, the instability sets in at a lower speed. As the area of the wing is increased, the divergence and flutter speeds are found to decrease as shown in Figs. 5 and Fig. 9, respectively. The greater the area of the wing, the greater the unsteady aerodynamic forces acting on it, causing the aeroelastic instability to occur at a lower speed. The analytical sensitivity gives a good linear approximation of the critical speeds over the range the aspect ratio and area of the wing are varied.

The divergence speed of the wing is found to decrease at first and then increase as the taper ratio is increased in Fig. 6. The linear approximation given by the analytical sensitivity appears to be bad as one moves away from the baseline. However, note that the divergence speeds lie in a narrow band between 137–140 m/s when the taper ratio is varied from 0.3 to 0.7. The flutter speed of the wing decreases as the taper ratio is increased as shown in Fig. 10. The flutter speed curve can be approximated linearly as indicated by the sensitivity prediction.

It can be seen from Fig. 7 that the divergence speed increases as the wing is swept backwards. The flutter speed decreases with increasing sweep angle about the 15 deg swept configuration as seen from Fig. 11, though the values of speed do not change much within the range of sweep angles plotted (10–20 deg). Fig. 3 gives a plot of flutter speeds for a higher range of sweep angles, for the same wing, where it can be seen that, though the flutter speed decreases with increasing sweep for lower sweep angles, it increases with sweep for higher sweep angles. By performing one sensitivity calculation at the baseline analytically, this method gives a linear

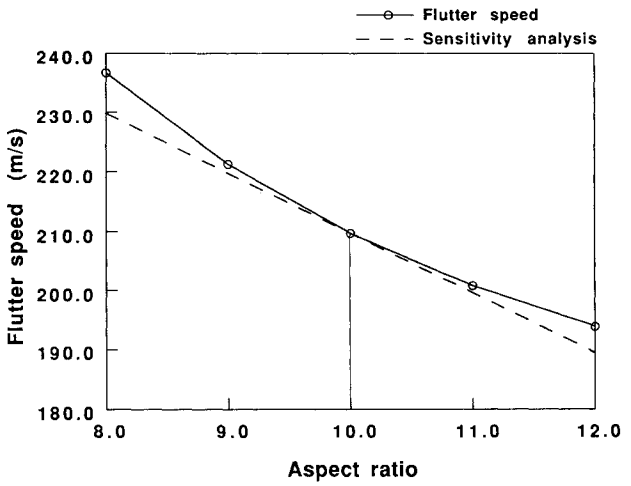

Fig. 8 Flutter speed vs aspect ratio ($M = 0.9$), aspect ratio = 10, area = 20 m^2, taper ratio = 0.5, sweep = 15 deg.

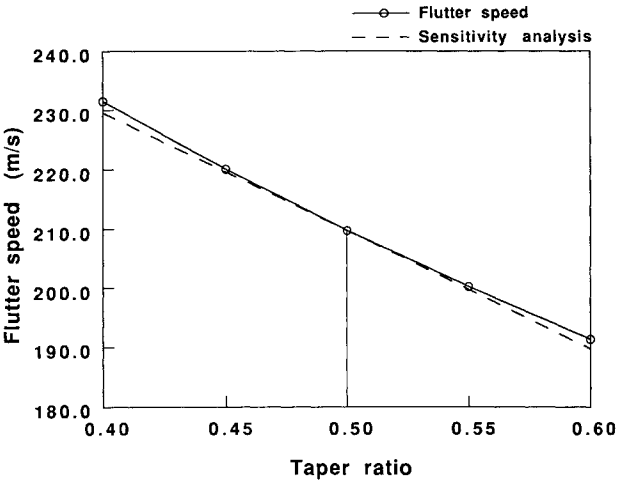

Fig. 10 Flutter speed vs taper ratio ($M = 0.9$), aspect ratio = 10, area = 20 m^2, taper ratio = 0.5, sweep = 15 deg.

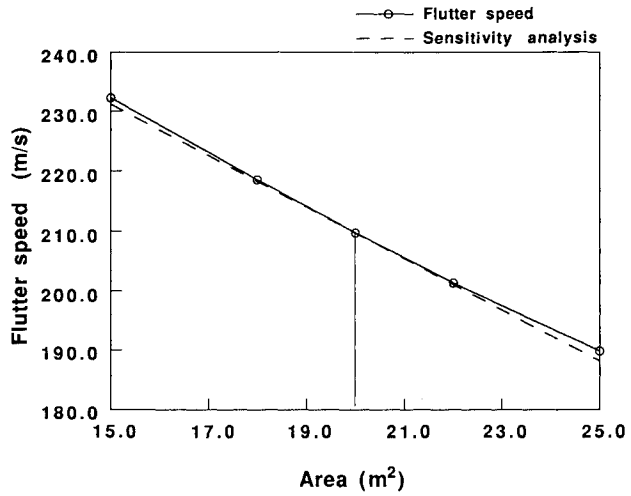

Fig. 9 Flutter speed vs area ($M = 0.9$), aspect ratio = 10, area = 20 m^2, taper ratio = 0.5, sweep = 15 deg.

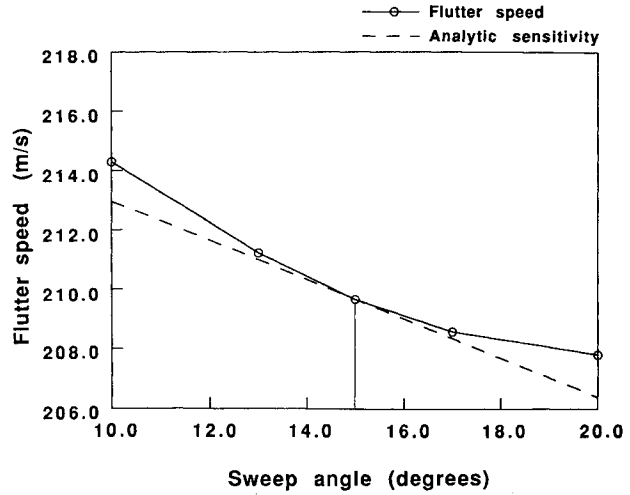

Fig. 11 Flutter speed vs sweep angle ($M = 0.9$), aspect ratio = 10, area = 20 m^2, taper ratio = 0.5, sweep = 15 deg.

Table 3 Sensitivity of divergence speed of the wing at $M = 0.9$ with respect to shape parameters[a]

Sweep angle, deg	Divergence speed, m/s	Parameter	Analytic derivative	Finite difference derivative		
				1.0%[b]	0.1%	0.01%
0	137.41	Aspect ratio	−4.9672	−4.9276	−4.9630	−4,9642
		Area	−4.2460	−4.2156	−4.2418	−4.2433
		Taper ratio	7.2069	7.4086	7.2601	7.2308
		Sweep ratio	147.0488	147.1087	147.2050	148.5662
15	203.74	Aspect ratio	16.9889	17.4989	17.0278	16.9773
		Area	−18.3916	−17.9050	−18.3307	−18.3768
		Taper ratio	440.3419	451.3756	441.1370	440.0515
		Sweep angle	434.5355	437.5666	434.5507	434.0796

[a]Area = 20 m^2, aspect ratio = 10, taper ratio = 0.5.
[b]Indicates step size.

Table 4 Sensitivity of flutter speed of the wing at $M = 0.9$ with respect to shape parameters[a]

Sweep angle, deg	Divergence speed, m/s	Parameter	Analytic derivative	Finite difference derivative	
				0.1%[b]	0.01%
0	229.90	Aspect ratio	−12.6812	−12.6675	−12.6779
		Area	−6.4607	−6.4563	−6.4592
		Taper ratio	−184.8167	−184.7288	−184.7691
		Sweep ratio	−104.4327	−104.3587	−104.4143
15	209.67	Aspect ratio	−10.1067	−10.0929	−10.1005
		Area	−4.3196	−4.3181	−4.3170
		Taper ratio	−199.1987	−199.1011	−199.0925
		Sweep ratio	−37.7435	−37.6769	−37.5526
30	213.22	Aspect ratio	−6.6440	−6.6311	−6.6404
		Area	−5.0568	−5.0542	−5.0554
		Taper ratio	−172.6965	−172.6105	−172.6414
		Sweep angle	67.8415	67.9632	67.8975

[a]Area = 20 m^2, aspect ratio = 10, taper ratio = 0.5.
[b]Indicates step size.

approximation to the critical speeds of the wing for changes in the wing shape parameters about the baseline. This information is useful for preliminary design purposes as it avoids the necessity of a reanalysis for small changes in any of the shape parameters.

Concluding Remarks

The compressible unsteady aerodynamic theory using indicial response functions was successfully used to represent the aerodynamic forces and moments on a finite-span wing. A constant value of the section lift-curve slope was used in the analysis. Using this aerodynamic, state-space model and the structural formulation based on Ritz technique, aeroelastic analysis of wings were carried out in transonic flow. The use of Chebyshev polynomials for Ritz functions gives the added benefit of closed-form analytical expressions for the derivatives of stiffness and mass matrices with respect to the shape design parameters of the wing. This avoids the uncertainities and the computational expense associated with finite difference derivative calculations. The shape sensitivity derivatives of the critical speed of the wing were computed by analy-tical and finite difference methods and they are in excellent agreement with each other. These shape derivatives of the aeroelastic response of a wing in transonic flow would be very useful to a designer in the initial design phase, thus avoiding the necessity of a reanalysis for small changes in the design parameters.

Acknowledgments

The work presented here is a part of the work done in the project sponsored by NASA Langley Research Center under Grant NAG-1-1411 to Virginia Polytechnic Institute and State University. We are thankful to J-F. M. Barthelemy, NASA Langley, for the fruitful discussions we have had with him.

References

[1]Leishman, J. G., and Nguyen, K. Q., "State-Space Representation of Unsteady Airfoil Behavior," *AIAA Journal*, Vol. 28, No. 5, 1990, pp. 836–844.

[2]Leishman, J. G., and Crouse, G. L., "Transonic Aeroelasticity Analysis Using State-Space Unsteady Aerodynamic Modelling," *Journal of Aircraft*, Vol. 29, No. 1, 1992, pp. 153-160.

[3]Sobieszczanski-Sobieski, J., "A System Approach to Aircraft Optimization," AGARD Rept. 784, Feb. 1992, pp. 2-1–2-15.

[4]Livne, E., "Analytic Sensitivities for Shape Optimization in Equivalent Plate Structural Wing Models," *Journal of Aircraft* (to be published).

[5]Rudisill, C. S., and Bhatia, K. G., "Optimization of Complex Structures to Satisfy Flutter Requirements," *AIAA Journal*, Vol. 9, No. 8, 1971, pp. 1486–1491.

[6]Pedersen, P., and Seyranian, A. P., "Sensitivity Analysis for Problems of Dynamic Stability," *International Journal of Solids and Structures*, Vol. 19, No. 4, 1983, pp. 315–335.

[7]Hawk, D. J., and Bristow, D. R., "Development of MCAERO Wing Design Panel Method with Interactive Graphics Module," NASA CR-3775, 1984.

[8]Yates, E. C., "Aerodynamic Sensitivity from Subsonic, Sonic and Supersonic Unsteady, Nonplanar Lifting Surface Theory," NASA TM-100502, 1987.

[9]Barthelemy, J.-F. M., and Bergen, F. D., "Shape Sensitivity Analysis of Wing Static Aeroelastic Characteristics," NASA TP-2808, May 1988.

[10]Kapania, R. K., "Sensitivity Analysis of Dynamic Aeroelastic Responses," AGARD Rept. 784, Feb. 1992, pp. 3-1–3-12.

[11]Kapania, R. K., Bergen, F. D., and Barthelemy, J.-F. M., "Shape Sensitivity Analysis of Flutter Response of a Laminated Wing," *AIAA Journal*, Vol. 29, No. 4, 1991, pp. 611–612; also NASA-CR-181725, Oct. 1988.

[12]Issac, J. C., and Kapania, R. K., "Sensitivity Analysis of Dynamic Aeroelastic Responses in Transonic Flow," Dept. of Aerospace Engineering, Virginia Polytechnic Inst. and State Univ., Blacksburg, VA, 1993; also AIAA Paper 93-1646, April 1993.

[13]Kapania, R. K., and Singhvi, S., "Free Vibration Analysis of Generally Laminated Tapered Skew Plates," *Composites Engineering*, Vol. 2, No. 3, 1992, pp. 197–212.

[14]Singhvi, S., and Kapania, R. K., "Analysis, Shape Sensitivities and Approximations of Modal Response of Generally Laminated Tapered Skew Plates," Center for Composite Materials and Structures Rept., Virginia Polytechnic Inst. and State Univ., Blacksburg, VA, Sept. 1991.

[15]Dugundji, J., and Landsberger, B. J., "Experimental Aeroelastic Behavior of Unswept and Forward Swept Cantilever Graphite Epoxy Wings," *Journal of Aircraft*, Vol. 22, No. 8, 1985, pp. 679-686.

[16]Yates, Jr., E. C., "AGARD Standard Aeroelastic Configurations for Dynamic Response. Candidate Configuration 1:—Wing 445.6," NASA TM 100492, Aug. 1987.